Hindawi
International Journal of Aerospace Engineering
Volume 2019, Article ID 8142532, 14 pages
https://doi.org/10.1155/2019/8142532

Research Article

Prediction of Heat Transfer Characteristics of the Carbonized Layer of Resin-Based Ablative Material Based on the Finite Element Method

Junjie Gao, Jijun Yu, Haitao Han, and Daiying Deng

China Academy of Aerospace Aerodynamics, Beijing 100074, China

Correspondence should be addressed to Haitao Han; han_ht@139.com

Received 17 March 2019; Revised 4 May 2019; Accepted 13 May 2019; Published 27 June 2019

Academic Editor: Marco Pizzarelli

The microstructure of the carbonized layer of the low-density resin-based ablative thermal insulation material is observed, and multiscale unit cell models are established for the residual carbon deposition mode of a carbonization process, and then the thermal conductivity coefficient is predicted using the finite element method. The heat transfer characteristics of a carbonized material are discussed and studied. The results show that among the several models established, the thermal conductivity coefficient obtained by the cross-linked model of matrix carbonization is more accurate, and the deviation compared with the experimental results is within 20%, which is more consistent with the actual heat transfer mechanism. At the same time, the finite element random model is used to predict the thermal conductivity coefficient. The results show that the deviation between the numerical results and the experimentally measured thermal conductivity coefficient of the carbonized layer is within 10%, showing that the accuracy of the finite element random model is significantly higher than that of the dual-scale unit cell model. The carbon deposition model can accurately predict the heat transfer characteristics of the carbonized layer.

1. Introduction

1.1. The Ablative Thermal Insulation Material. Ablative thermal insulation material often covers the surface of the air vehicle to keep the inner temperature steady. Figure 1 is the material specimen, and we can see that the surface of the specimen is different from the inner part. It is because the surface has been suffered from the aerodynamic heating of ground experiment. So the surface has become the loose layers of carbon, and it is different from the original layer.

Figure 2 shows the layered structure of a kind of ablative thermal insulation material called the PICA (Phenolic-Impregnated Carbon Ablator) [1]. The surface of the specimen is a carbonized layer, the back of the specimen is the original layer, and there is a transition area called the pyrolysis layer located between the carbonized layer and the original layer. The characteristic of the pyrolysis layer is very complicated because of the pyrolytic part and the original part mixed. The purpose of this article is to explore the heat transfer properties of the carbonized layer of the thermal insulation material.

1.2. Research Progress on Heat Transfer Characteristics. As for the mesoscopic heat transfer characteristics, generally, there are three methods: they are the theoretical method, empirical method, and finite element method.

For the theoretical method, the methods include the one-dimensional heat conduction method, serial and parallel structure method, and homogenization method, and they are used to calculate the coefficient of thermal conductivity of some composite materials [2–4].

For the empirical method, four empirical formulas were used to predict the effect of lamellar holes of fiber-reinforced composites on effective thermal conductivity; this work was done by Al-Sulaiman et al. [5].

For the finite element method, the focus was on the establishment of the unit cell model; the calculation process was to be done by the finite element method. Some scholars use this

(a) (b)

Figure 1: The specimen of ablative thermal insulation material: (a) vertical view (b) front view.

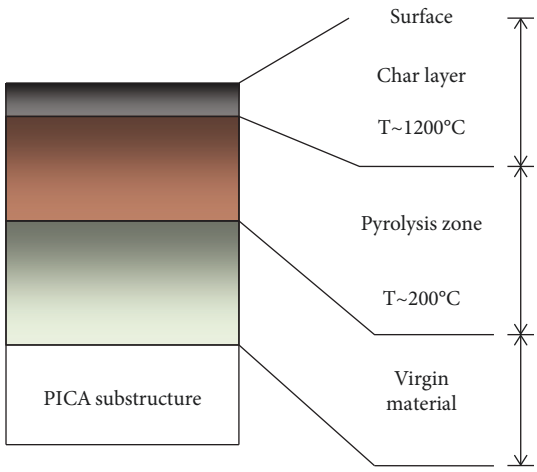

Figure 2: The layered structure of PICA material after surface ablation [1].

method to make prediction of the effective thermal conductivity of some composite materials such as ceramic matrix composites, braided composite material, and microsphere composite [6–8].

1.3. Research Progress on Microstructure Analysis of Carbonized Layers. In order to analyze the microstructure of carbonized layers, some scholars prepared a kind of insulation material called the EPDM (Ethylene-Propylene-Diene Monomer) and made some research about the microstructure of the original and carbonized layers [9–13]. Characterization facilities such as the SEM (scanning electron microscope), TEM (transmission electron microscope), and cone calorimeter were often used to study the microstructure of the thermal insulation material [14, 15].

Simulation methods were also used in the analysis of the carbonized layers. Through simulation methods, they can often acquire the carbonation rate, quality ablation rate, and the amount of carbon consumption and compare them with the experimental results [16, 17].

Existing research focuses more on the heat transfer characteristics of the thermal insulation material's original layer, for carbonized layers, focusing more on mechanical performance or the heat transfer and mechanical performance from the macroscopic scale.

In the authors' previous article "Prediction of Meso-Heat Transfer Characteristics of Resin-Based Ablative Materials" of the Chinese Journal of Aeronautics, the theoretical model of different scales and two-dimensional finite element random model were established to forecast the heat transfer characteristics, and the influence of mesoscopic parameters on the heat transfer characteristics was discussed. After external heating, the matrix and the wall of microspheres will all be carbonized and the carbonized matrix will be deposited on the surface of the microspheres, forming a very complicated and loose mesostructure. For the depositional mode and the heat transfer characteristic of carbonized layers, previous research was conducted. The heat transfer mechanism of the ablative thermal insulation material is very complicated; it includes the thermal conduction, thermal convection, and thermal radiation. In order to explore the relationship between the heat transfer characteristics and the mesostructure, here, we explore the heat transfer characteristics at room temperature, so we do not consider the thermal radiation. Skochdopole found in the experiment that for the hole whose diameter was less than 4 mm, there was no natural convection of the gas [18]. The pore size is very small; its equal diameter is far less than 4 mm, so we ignore the thermal convection. Exploring the heat transfer characteristic is very important because the carbonized ablator normally provides the most efficient thermal protection shield for the major portion of a manned entry vehicle [19]. So the depositional mode after carbonization and the heat transfer characteristic in mesoscopic scale at room temperature of the thermal insulation material are necessary to be studied.

2. Microstructure Investigation

The specimen in Figure 1 was acquired by a stagnation point test in a high-frequency induction heating wind tunnel, the heat flux is 370 kW/m^2, the gas total enthalpy is 6.5 MJ/kg, the stagnation pressure is 1700 Pa, and the time is 345 s.

In order to know what the microstructure of the ablative thermal insulation material is, we use the scanning electron microscope. First, we get several small pieces of samples

Figure 3: The sample to be observed.

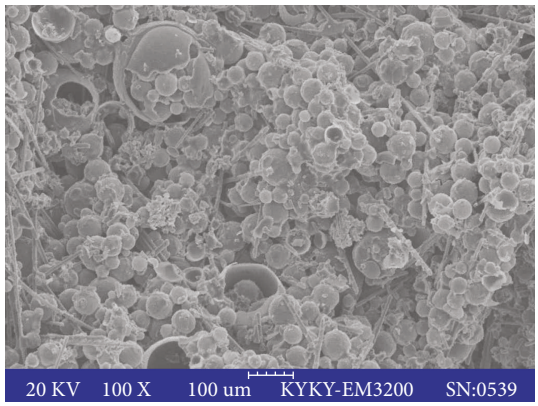

Figure 4: Microstructure image of the original ablative thermal insulation material.

containing both the original layer and the carbonized layer from the specimen in Figure 1 as shown in Figure 3. The sample includes the carbonized layer, the pyrolysis layer, and the original layer. The sample to be observed should be ultrasonically cleaned and dried. Then, we use the scanning electron microscope to get the microstructure image. As the scanning electron microscope needs a sample which is in good electrical conductivity and the ablative insulation material is nonconducting, so it should be gold planted firstly. Then, we get the microstructure image of the original and the carbonized layer, and they are separately shown in Figures 4 and 5.

It can be easily found that the microspheres of the original layer shown in Figure 4 are nearly complete and the microspheres of the carbonized layer shown in Figure 5 are broken. The broken microspheres of the carbonized layer are mainly caused by the ablation effect. It is not the reason of ultrasonic cleaning because both the original and the carbonized layer are all ultrasonically cleaned, and according the work of Li et al. [20], the surface of the carbonized layer is usually compact and can resist the airflow so the ultrasonic cleaning will not destroy the microspheres. On the other hand, Zhang et al. and He et al. [21, 22] study the alginate microspheres' mechanical properties through the ultrasonic effect, and the microspheres were not broken in the effect of the ultrasonic effect.

It can be seen from Figure 4 that the original ablative thermal insulation material includes phenolic hollow microspheres, fiber, and the phenolic resin matrix. And they are randomly distributed. The resin matrix makes the microspheres and fibers adhere to each other. After heating with high temperature, the phenolic will pyrolyze and convert into carbon. So the wall of the microspheres and the resin matrix will all convert into carbon, and their volume will shrink. As shown in Figure 6, the porosity increases significantly compared with the original layer. According to the microstructure image, the geometrical characteristics of the material components are statistically analyzed, including the distribution of the microsphere radius, fiber length, and fiber diameter.

We use the software of Image Pro Plus to analyze the mesoscopic size including the microsphere and the fiber. Figure 7 is the microsphere's outer radius distribution histogram of the carbonized layer; Figures 6 and 8 are the fiber length and fiber diameter distribution histogram, respectively. It can be seen that after carbonization, microspheres' outer radius, fiber length, and diameter are approximately in line with Gaussian distribution, which can be described as

$$y = a \exp\left[-\left(\frac{x-b}{c}\right)^2\right], \tag{1}$$

where x denotes the mesoscopic parameter such as the microsphere radius, fiber length, and fiber diameter and y is the distribution ratio. For the microsphere radius, the parameters in the formula are

$$\begin{aligned} a &= 38.63, \\ b &= 20.16, \\ c &= 6.884. \end{aligned} \tag{2}$$

For the fiber length, the parameters in the formula are

$$\begin{aligned} a &= 25.86, \\ b &= 214.5, \\ c &= 108.2. \end{aligned} \tag{3}$$

For the fiber diameter, the parameters in the formula are:

$$\begin{aligned} a &= 26.44, \\ b &= 9.512, \\ c &= 1.055. \end{aligned} \tag{4}$$

The fitting results of each size distribution and Gaussian function are shown in Figures 9–11, respectively.

After carbonization, the fraction of the residual carbon is 30% of the original material layer [23]. Each component's parameters of the original layer provided by the place where the materials are synthesized are shown in Table 1. The volume fraction is calculated by the mass fraction, the density, and the basic law of physics. The thermal conductivity

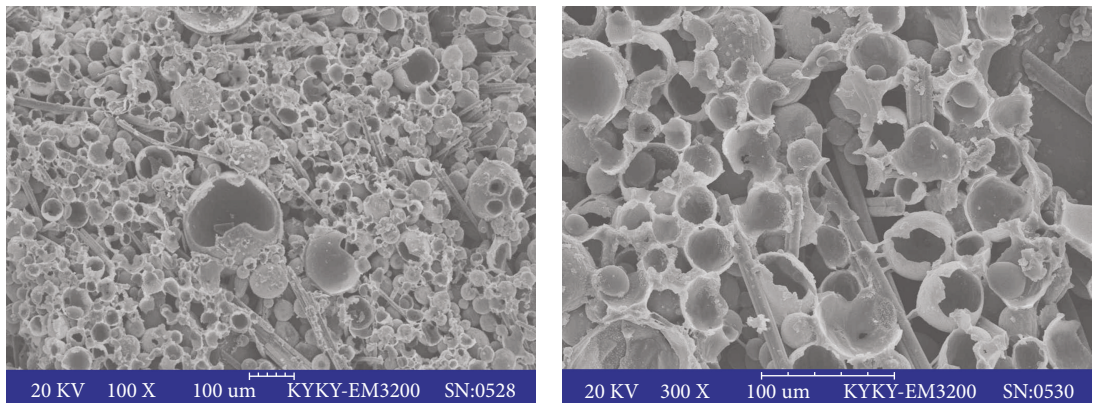

(a) (b)

Figure 5: Microstructure image of the carbonized layer of ablative thermal insulation material: (a) 100 times magnified image and (b) 300 times magnified image.

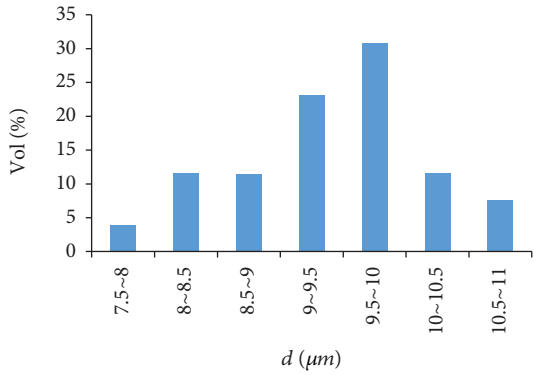

Figure 6: Fiber diameter distribution.

coefficient of each component is measured based on the plate method by the place where the materials are synthesized. A, B, and C are three kinds of ablation material which has the similar microstructure composition but have different proportions of each component.

According to the carbon residue rate and the data in Table 1, we can get the parameters of each component of the material after carbonization as shown in Table 2. The thermal conductivity values of each component in Table 2 are also provided by the place where the materials are synthesized.

3. Models and Analysis

As can be seen from Figures 6–8, the fiber length scale is bigger than the microsphere and pore scale by an order of magnitude. According to the concept of mesomechanics, the thermal performance can be analyzed by two different dimensional models, i.e., the microsphere scale model and the fiber scale model. The microsphere scale model consists of the matrix, microsphere, and pore, and the fiber scale model consists of the fibers and the equivalent material from the microsphere scale model for the thermal conductive analysis.

Figure 12 shows detailed structure images of the carbonized layer of a resin-based ablative material. From Figure 12(a), it can be seen that small carbon particles form after carbonization of the matrix and are deposited on microspheres or mixed with them. From Figure 12(b), it can be seen that a part of the carbonized matrix was deposited on the surface of microspheres and another part cross-link between them; the rest of matrix was deposited on the surface of fibers.

Figure 13 shows the structure of the carbonization layer and the deposition mode of the EPDM insulation material clearly. The carbonization layer is the first barrier against the ablation of insulation materials, so it is the first to be subjected to thermal-chemical ablation and particle and gas-mechanical erosion [20]. The carbonization layer usually has a compact surface which is formed by redeposition which is initially porous. And the rest of the carbonization layer is usually porous. However, compared to the porous carbonization layer, the compact surface is very thin, which can be seen clearly in Figure 13.

On the basis of these analyses, several kinds of the carbon deposition model can be set up.

3.1. Models of Microsphere Scale. From the mesoscopic structure image of Figures 5 and 12, it can be seen that after carbonization, the resin matrix pyrolyzes and its volume shrinks. In most of the carbonized matrix deposit between microspheres, a small number of matrix were deposited on the surface of fibers. The heat transfer characteristics will be studied by three carbon deposition models.

3.1.1. Wrapper Model. Assume that the matrix is completely attached to the microspheres after carbonization, and the microspheres are changed into new microspheres with a thicker wall; the unit cell model is shown in Figure 14.

For this model, the finite element method is used for the computation of the equivalent coefficient of thermal conductivity. Due to the same heat transfer characteristics along the three-axis direction of this model, here, we can calculate the equivalent coefficient of thermal conductivity along the y direction. In loading temperature boundary condition and periodic boundary condition, we can get the quantity of heat

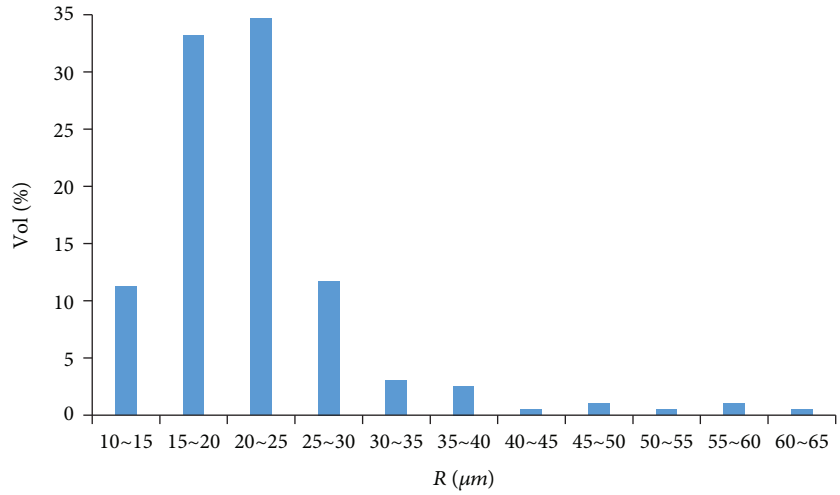

Figure 7: External radius distributions of the carbonized layer's microsphere.

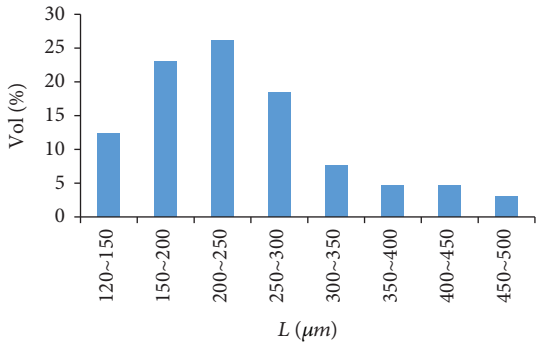

Figure 8: Fiber length distribution.

which gets through a plane perpendicular to the y direction; then we can use the Fourier's law to calculate the equivalent coefficient of thermal conductivity. The temperature contours and the heat flux vector diagram are shown in Figures 15 and 16, and temperature and heat flux profile are shown in Figures 17 and 18. The origin of the coordinate is the center point of the calculation domain, and it is the same for the following figures in this article. The profile of Figures 17 and 18 is the plane of $z = 0$ in Figures 15 and 16 separately. And it is the same for the following profile figures.

Due to considering the matrix completely deposited on the microspheres, the heat between microspheres is transferred by the air in the pore which has a lower thermal conductivity coefficient; the heat transfer process can be clearly seen in Figure 18 that most thermal flux transfers through the wall of microspheres.

3.1.2. Crosslinked Model. Consider that the carbon matrix makes the microspheres crosslink and lets the heat transfer between microspheres. Figure 19 is the representative volume element of the crosslinked model, and Figure 20 is the unit cell of the crosslinked model.

The unit cell model is set up using the finite element method, and by loading temperature and periodic boundary conditions, we get the results. Figures 21 and 22 are, respectively, the temperature contours and the heat flux vector diagram. It can be seen that more quantity of heat transfers through the microsphere wall and the matrix between them. There is less heat transfer through other parts. In order to more clearly see the internal heat transfer, we make cross-section images as shown in Figures 23 and 24. Because of the difference of the thermal conductivity coefficients between the air and the material of the microsphere wall and matrix, it leads to the isotherm distribution in Figures 23 and 24 which clearly shows the heat transfer condition; that is, most of the heat transfers through the microspheres and the matrix which were carbonized.

3.1.3. Microsphere Carbonization Model. Here, we consider the carbonized matrix deposits on fibers. In the microsphere scale, only the wall of microspheres is carbonized, and Figure 25 shows its unit cell model.

The unit cell model is established using the finite element method, and by loading temperature and periodic boundary conditions, we get the results. Figures 26 and 27 are, respectively, the temperature contours and the heat flux vector diagram, and Figures 28 and 29 are, respectively, the temperature profile contours and the heat flux vector profile. It can be seen that as the heat is transferred through the air between microspheres, the heat transferred is much less.

Table 3 shows the prediction results of the thermal conductivity coefficient of the microsphere scale models. It can be seen that the thermal conductivity coefficient of wrapper model and microsphere carbonization model are less than the crosslinked model. It is because in the two models, the heat transfers through the air and, in the crosslinked model, the heat transfers through the matrix between microspheres, so it has the bigger thermal conductivity coefficient.

3.2. Models of Fiber Scale

3.2.1. Fiber Scale Model of Wrapper. For the fiber scale model, as a result of the random characteristics of the fiber orientation, length, and the distribution, here, we use the finite element model of fiber random distribution. We use the uniformly distributed model to simulate the location, the

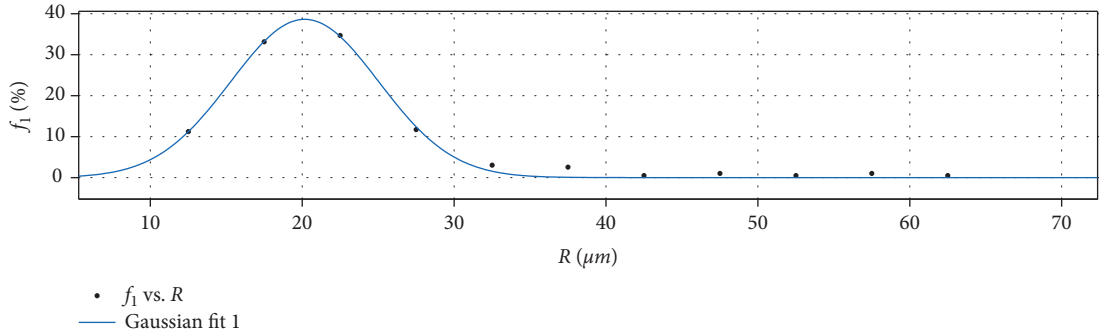

Figure 9: Data fitting result of pore size distribution of the carbonized layer's microsphere.

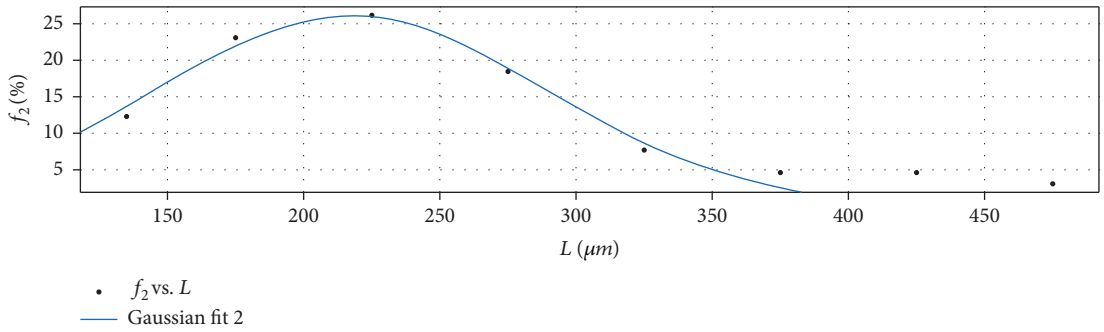

Figure 10: Data fitting result of fiber length distribution.

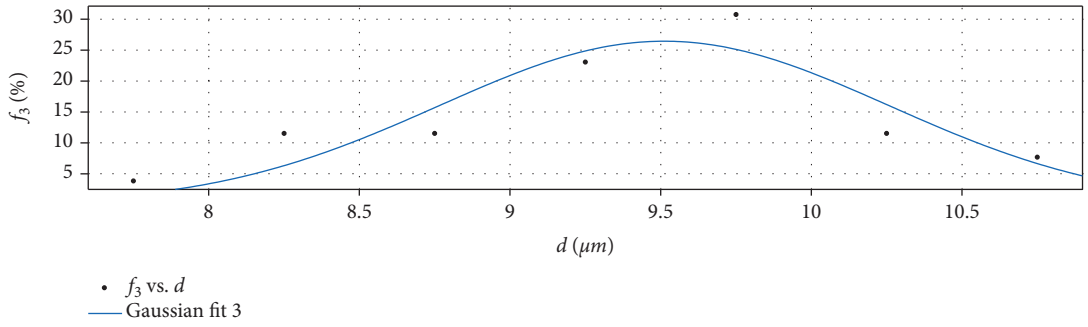

Figure 11: Data fitting result of fiber diameter distribution.

Table 1: Each component's parameters of the ablation material's original layer.

Component	Volume fraction (%) A	B	C	Thermal conductivity coefficient ($W \cdot m^{-1} \cdot K^{-1}$)
Phenolic matrix	21.57	43.16	28.61	0.2
Silica fiber	0.06435	0.2323	0	0.6
Carbon fiber	0	0	0.7084	40
Microsphere	33.74	38.16	33.05	0.2
Poriness	44.63	18.45	37.63	0.023

Table 2: Each component's parameters of the ablation material's carbonized layer.

Component	Volume fraction (%) A	B	C	Thermal conductivity coefficient ($W \cdot m^{-1} \cdot K^{-1}$)
Carbon matrix	4.67	9.35	6.2	16
Silica fiber	0.0644	0.2323	0	0.6
Carbon fiber	0	0	0.7084	40
Microsphere	26.62	30.11	26.08	16
Poriness	68.64	60.3	67.01	0.023

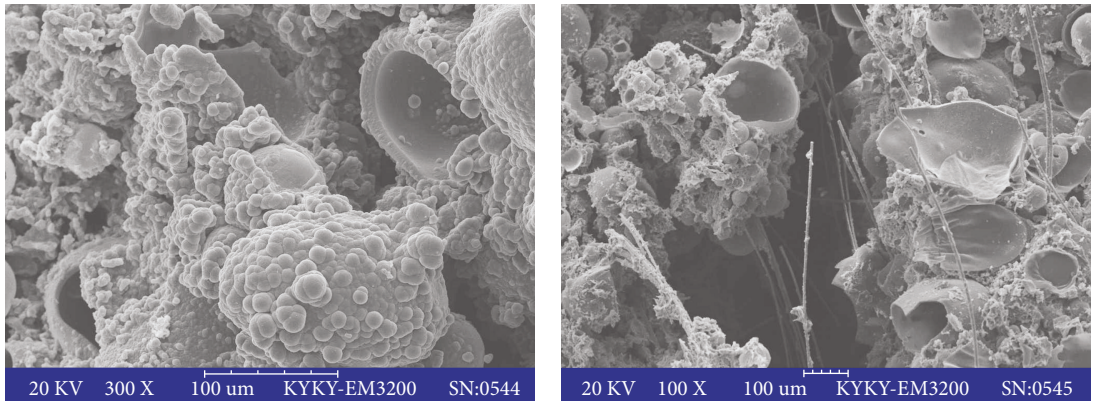

(a) (b)

Figure 12: Carbon deposited image of the resin matrix ablation material's carbonized layer: (a) 300 times magnified image and (b) 100 times magnified image.

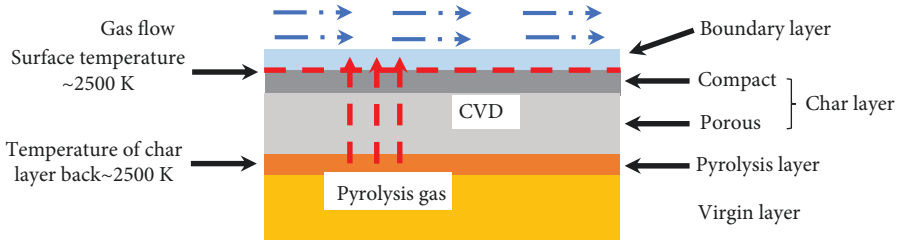

Figure 13: Schematic of the formation mechanism of the compact layer [20].

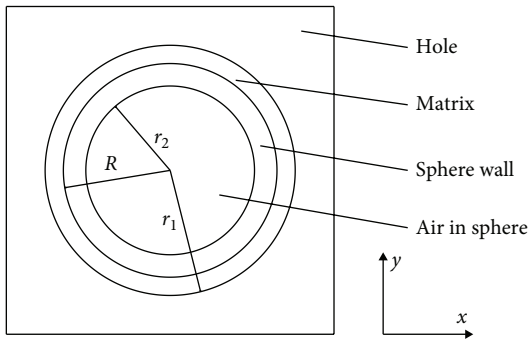

Figure 14: Model of carbon matrix deposit on the microsphere.

length, and the orientation of fibers. The temperature boundary condition and periodic boundary condition are loaded to get the result. For the sake of accuracy, we calculate each model five times and get the average result. The temperature contours and the heat flux vector diagram are shown in Figures 30 and 31, respectively.

3.2.2. Fiber Scale Model of Crosslinked. For the crosslinked model of the fiber scale, the finite element model of fiber random distribution is also used, it is the same with that in Section 3.2.1, and the results will be listed later.

3.2.3. Fiber Scale Model of Depositing on Fibers. For the model of matrix depositing on fibers, we assume that the matrix evenly wraps fibers, so when heat transfers along the fiber direction, as shown in fiber 1 in Figure 32, it is the parallel model of the fiber and the matrix. When heat transfer is perpendicular to the fiber direction, as shown in fiber 3 in Figure 32, it is the series model. The actual fiber direction and the heat transfer direction are at a certain angle, such as θ; due to the random fiber orientation, here, we can take an average concept, namely, the parallel model and the series model half and half. Then the new equivalent thermal conductivity coefficient of fibers can be gotten and the finite element model in which the fibers randomly distribute can be established.

The volume fraction of the carbonized matrix and fiber in the material are, respectively, φ_{m0} and φ_{f0}; the percentage of the total volume of the carbonized matrix and fiber is

$$\varphi_m = \frac{\varphi_{m0}}{\varphi_{m0} + \varphi_{f0}}, \qquad \varphi_f = \frac{\varphi_{f0}}{\varphi_{m0} + \varphi_{f0}}. \tag{5}$$

The thermal conductivity of the fibers adhering to the carbonized matrix is [24, 25]

$$k_{f1} = \frac{k_f k_m}{2\left(\varphi_f k_m + \varphi_m k_f\right)} + \frac{\varphi_f k_f + \varphi_m k_m}{2}. \tag{6}$$

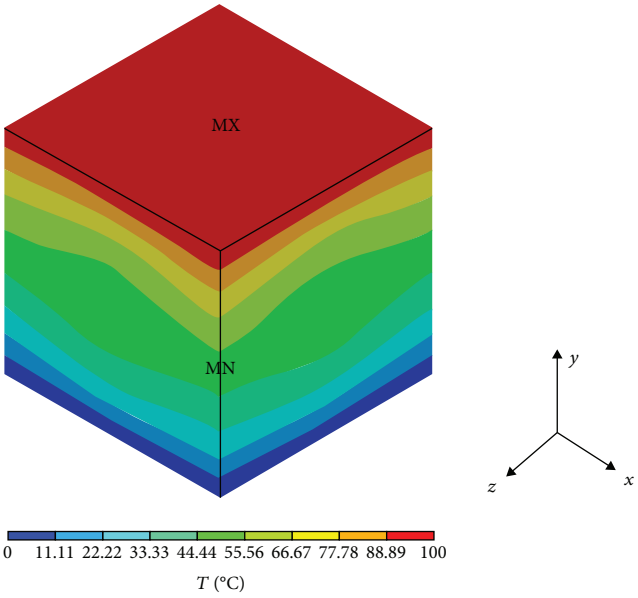

Figure 15: Temperature distribution of the wrapper model.

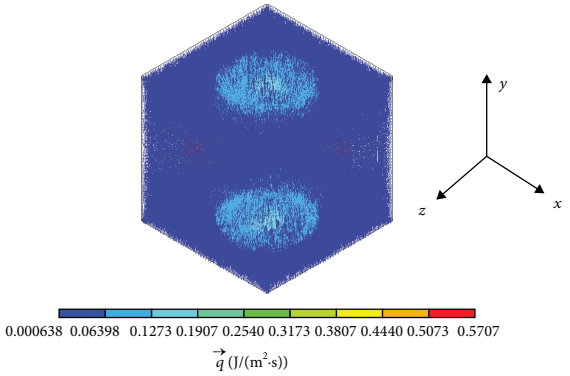

Figure 16: Heat flow vector of the wrapper model.

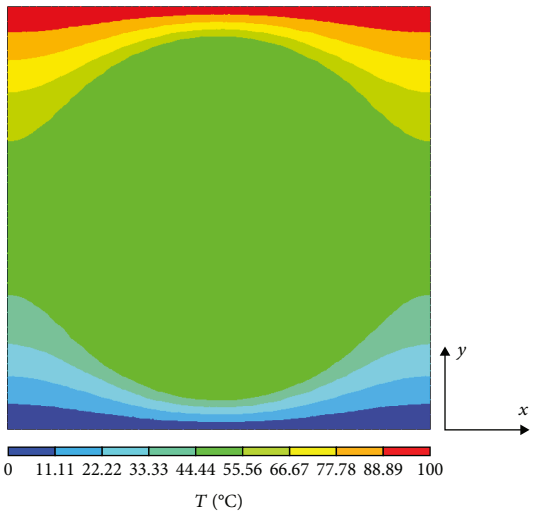

Figure 17: Profile image of the temperature distribution of the wrapper model.

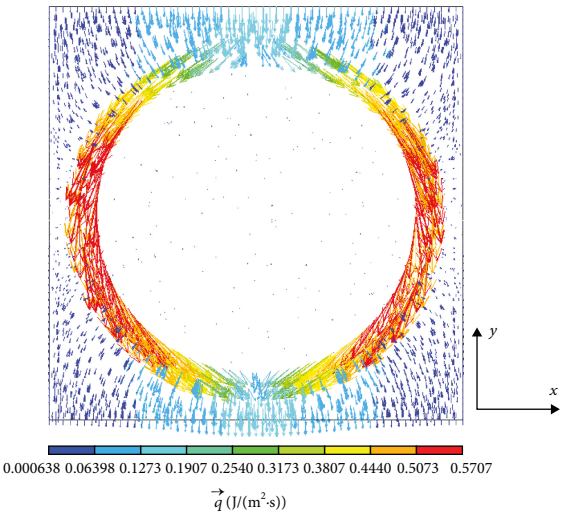

Figure 18: Profile image of the heat flow vector of the wrapper model.

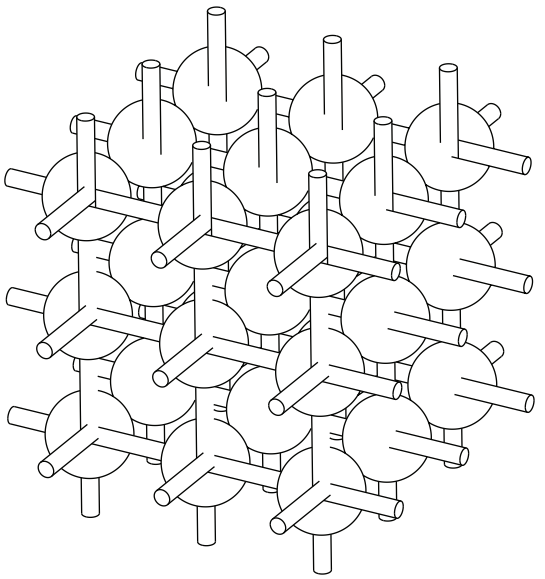

Figure 19: Crosslinked model.

The two diameters are, respectively, recorded as r_{f2} and r_{f1}, the length of the fiber is l_f, and the volume of the single cell is V. Then,

$$\begin{aligned} \pi r_{f1}^2 l_f &= V\varphi_f, \\ \pi r_{f2}^2 l_f &= V\left(\varphi_f + \varphi_m\right). \end{aligned} \tag{7}$$

The ratio of the fiber diameter adhering to the matrix and the original is

$$\frac{r_{f2}}{r_{f1}} = \sqrt{1 + \frac{\varphi_m}{\varphi_f}}. \tag{8}$$

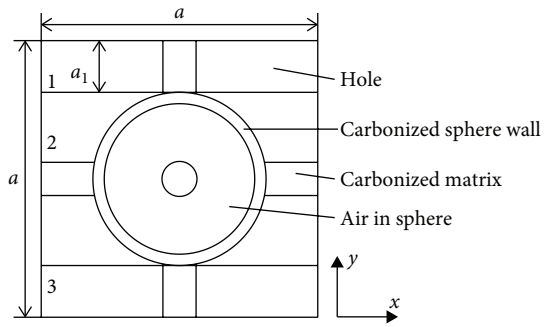

Figure 20: Unit cell of the crosslinked model.

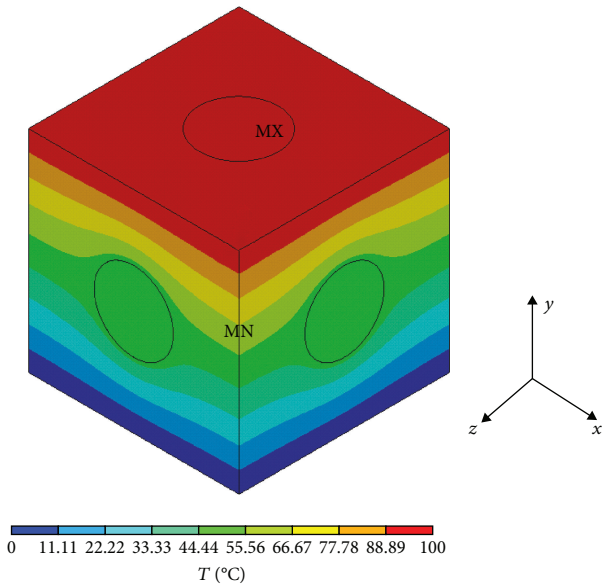

Figure 21: Temperature distribution of the crosslinked model.

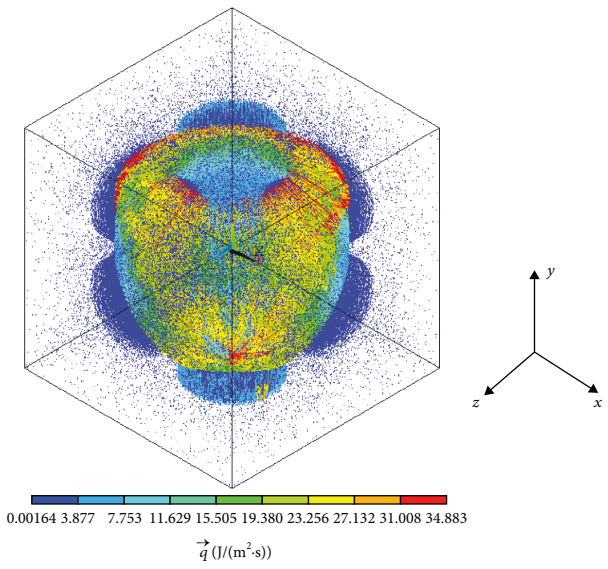

Figure 22: Heat flow vector of the crosslinked model.

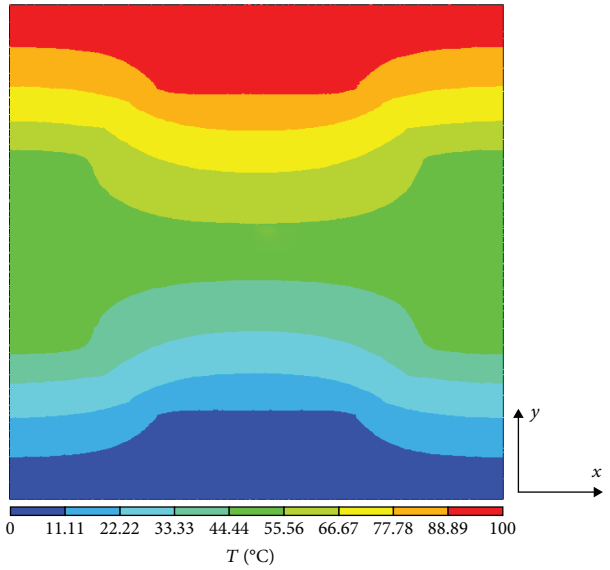

Figure 23: Profile image of the temperature distribution of the crosslinked model.

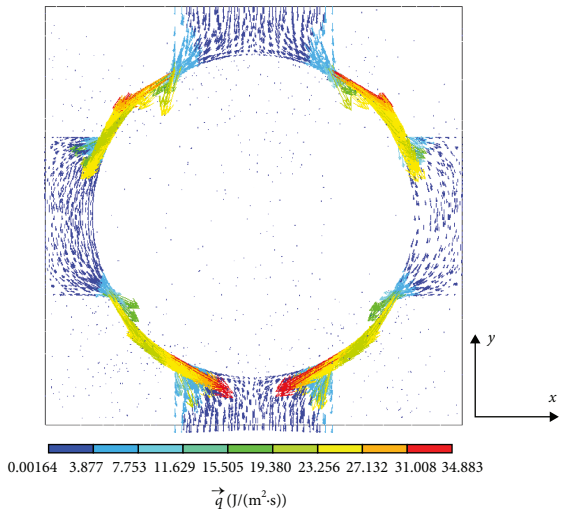

Figure 24: Profile image of the heat flow vector of the crosslinked model.

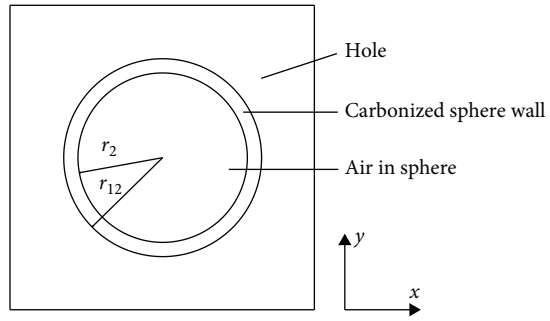

Figure 25: Microsphere carbonization model.

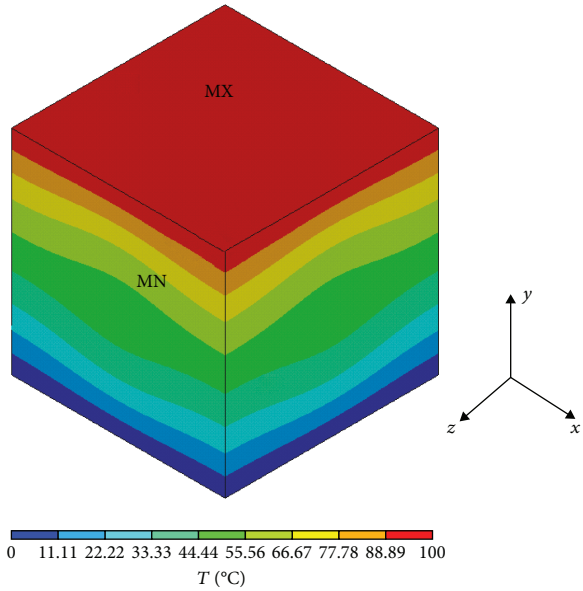

Figure 26: Temperature distribution of the microsphere carbonization model.

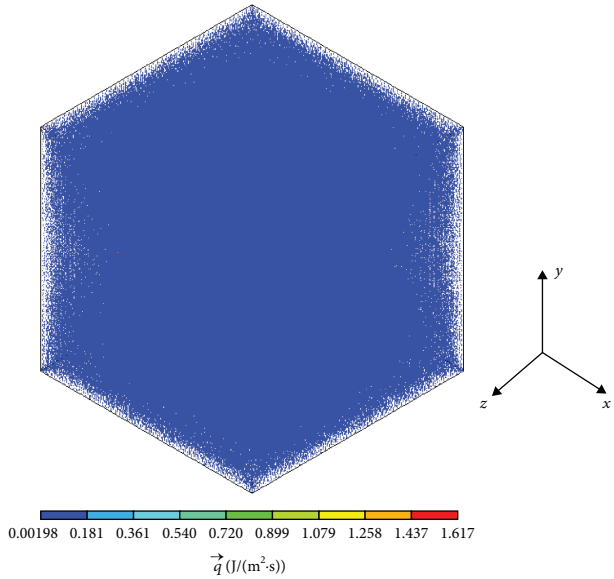

Figure 27: Heat flow vector of the carbonization model microsphere.

Thus, in the new finite element calculation of the fiber scale, the length parameters are the same statistical results as before, and fiber diameter parameters are the calculated results above. Then, the random model of the finite element is established and loaded the temperature boundary condition and periodic boundary condition. For the sake of accuracy, we calculate each model five times and get the average result. The temperature contours and the heat flux vector diagram are shown in Figures 33 and 34, respectively.

The prediction and the experiment thermal conductivity results of the three fiber scale models were compared, as shown in Table 4.

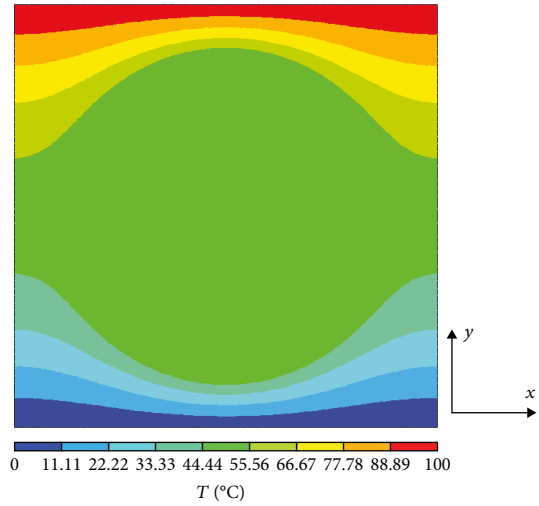

Figure 28: Profile image of the temperature distribution of the microsphere carbonization model.

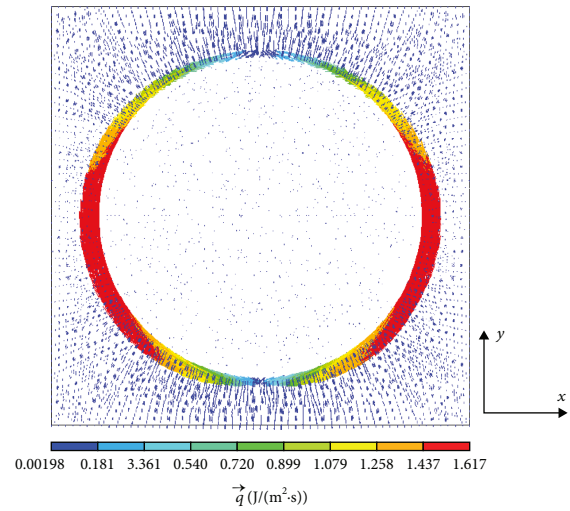

Figure 29: Profile image of the heat flow vector of the microsphere carbonization model.

Table 3: Thermal conductivity coefficient of microsphere dimension.

Model type	Thermal conductivity coefficient ($W \cdot m^{-1} \cdot K^{-1}$)		
	A	B	C
Deposit on microsphere	0.05442	0.07162	0.05626
Crosslinked model	0.3730	0.4720	0.4309
Microsphere carbonization	0.04591	0.05038	0.04526

As can be seen from Table 4, for the three types of carbon deposition model, the result of the crosslinked model is agreed well with the measured results and the deviation of the measured values, as shown in Table 5, is within 20%. And the other two prediction results are tiny. It is indicated that the crosslinked model is a reasonable carbon deposition way which is consistent with the heat transfer mechanism of the material.

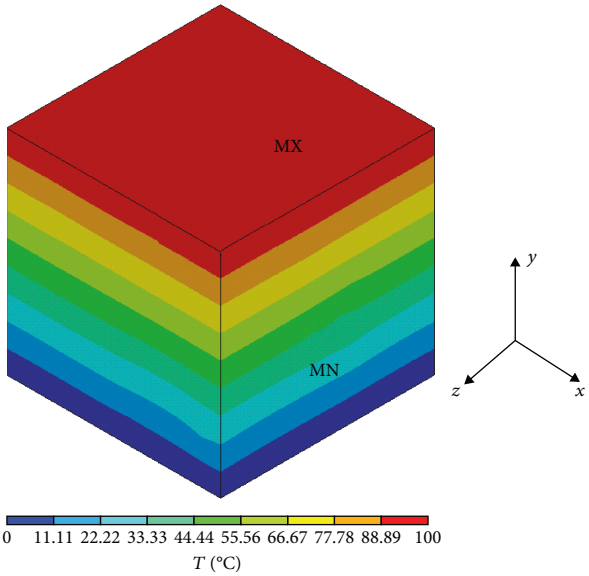

Figure 30: Temperature distribution of the fiber scale model of the wrapper.

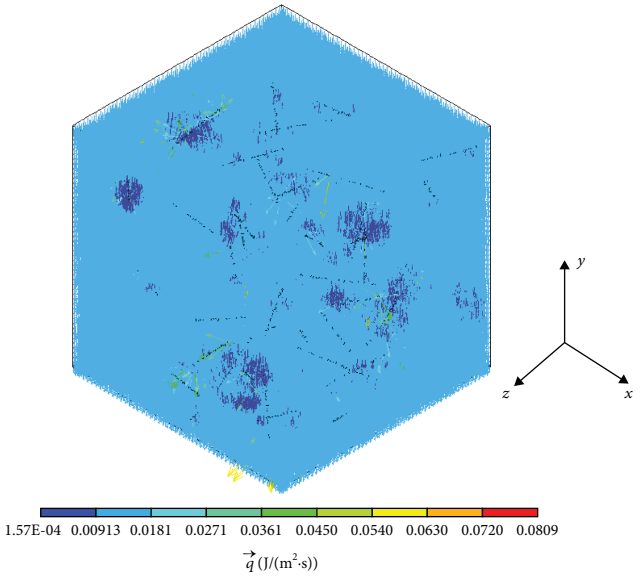

Figure 31: Heat flow vector of the fiber scale model of the wrapper.

3.3. Finite Element Random Model. Due to the reason of the material technology, the components in the microscopic structure of the actual carbonized layer are randomly distributed, as shown in Figure 5. According to the foreword, we can see that the thermal conductivity coefficient result of the crosslinked model agrees well with the experimental results. Then, in the finite element random model, we use the crosslinked mechanism.

Based on the microstructure statistical parameters, the finite element random model was established and loaded the temperature boundary condition and periodic boundary condition. For the sake of accuracy, we calculate each model five times and get the average result. The temperature contours and heat flux vector diagram are shown in Figures 35 and 36, respectively. The corresponding temperature profile contours and the heat flux vector profile are shown in Figures 37 and 38, respectively. It can be seen that the heat transfers mainly through the carbonized matrix and the microsphere wall, and the rest of the heat transferring is less. It can be more clearly seen from Figure 38 that microspheres which are closer to each other are connected by the carbonized matrix, so the thermal flux mainly transfers through the wall of microspheres and the carbonized matrix between them.

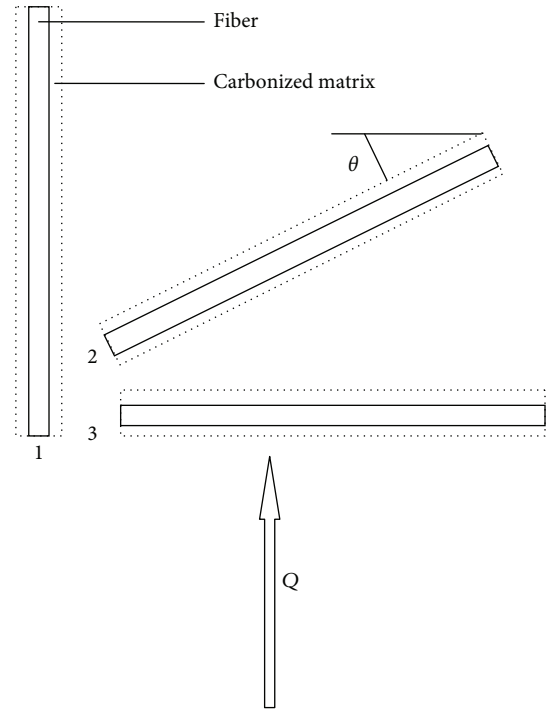

Figure 32: Model of depositing on the fiber with carbon.

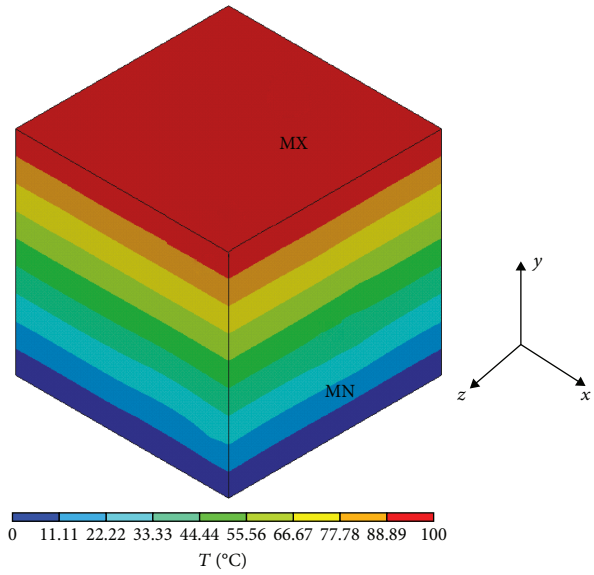

Figure 33: Temperature distribution of depositing on the fiber with the carbon model.

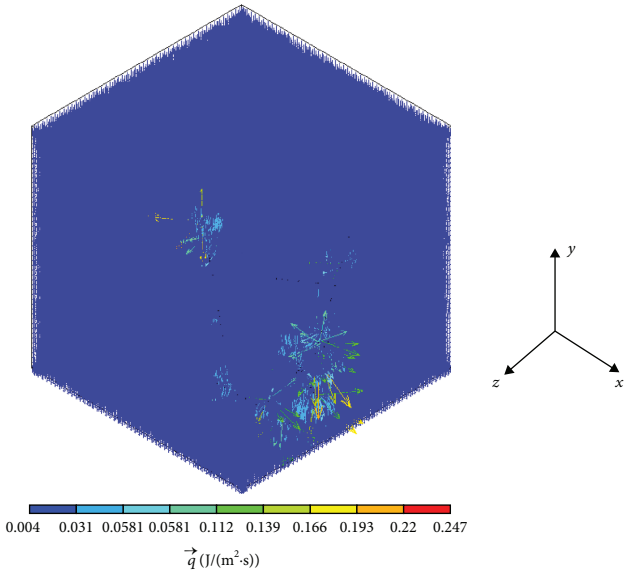

Figure 34: Heat flow vector of depositing on the fiber with the carbon model.

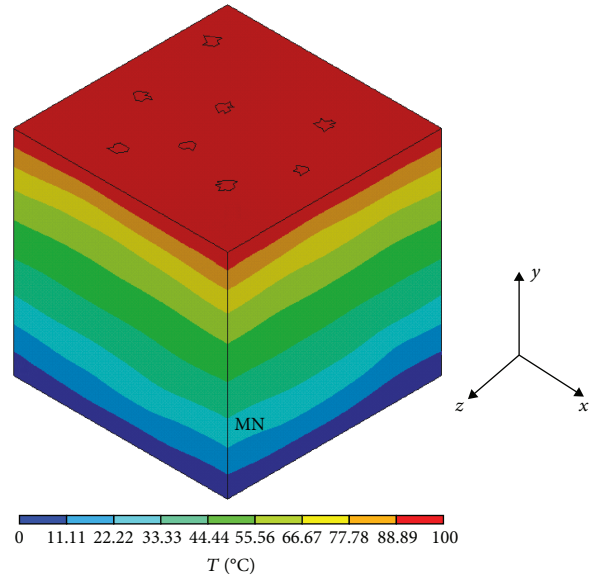

Figure 35: Temperature distribution of the finite element random model.

Table 4: Thermal conductivity coefficient of fiber dimension.

Model type	Thermal conductivity coefficient ($W \cdot m^{-1} \cdot K^{-1}$)		
	A	B	C
Deposit on microsphere	0.05475	0.07347	0.05774
Crosslinked model	0.3734	0.4806	0.4391
Microsphere carbonization	0.04624	0.05097	0.04574
Experiment result	0.45	0.423	0.5

Table 5: Comparison between the crosslinked model and experimental result.

Material type	A	B	C
Deviation (%)	17.02	13.62	12.18

The results of the finite element random model and the experiment are shown in Table 6. As can be seen, for the carbonized layer of the three kinds of resin-based ablative material, the deviation of the thermal conductivity coefficient between the prediction results and the experimental results is within 10%, which indicates that the established finite element random model can accurately predict the heat transfer characteristics of the carbonized layer.

4. Conclusions

In this paper, the heat transfer characteristics of the carbonized layer of the resin-based ablative material are investigated from two scales. Three numerical models based on unit cell representation are developed, and the thermal conductivity coefficients are gotten by finite element methods. The prediction results have been compared with the experimental results showing that the crosslinked model of the microsphere scale well coincides with the experimental results. This work is very meaningful for the investigation of the carbon deposition and heat transfer characteristics of the carbonized layer of the thermal insulation material. And as the thermal conductivity coefficient of the carbonized layer cannot be easily measured, the rapid prediction result can give a relatively accurate estimation. It can be meaningful for the material process design.

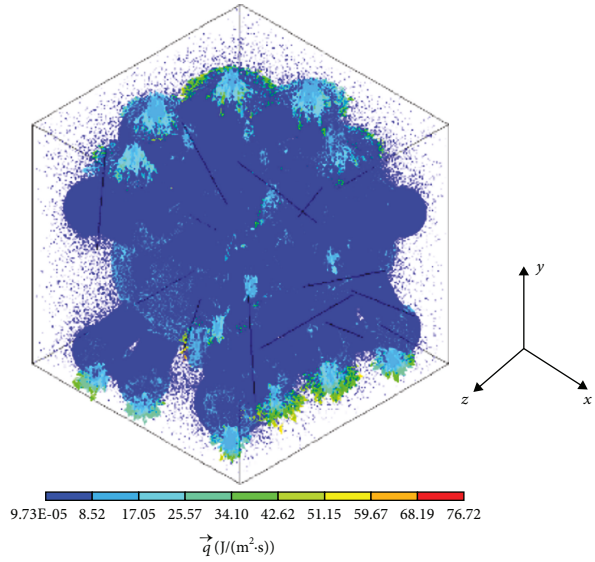

Figure 36: Heat flow vector of the finite element random model.

The main conclusions from this work can be summarized as follows:

(1) After carbonization, the matrix of the resin-based ablative material is mainly deposited between microspheres, and the others are deposited on fibers

(2) The carbonized matrix between microspheres is mainly responsible for the heat transfer of the carbonized layer

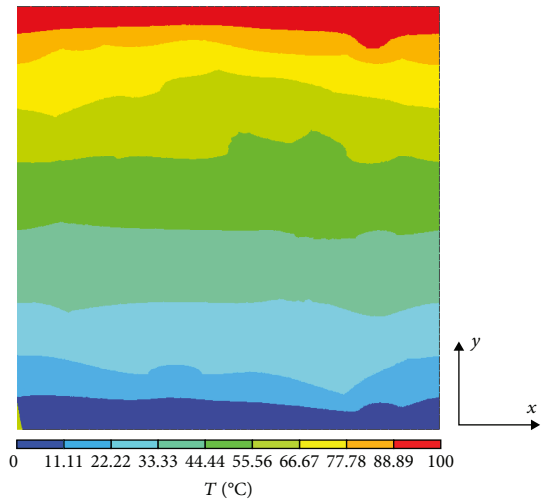

Figure 37: Profile image of the temperature distribution of the finite element random model.

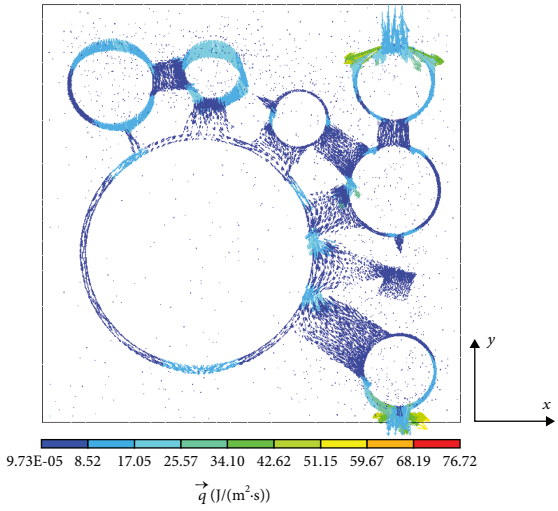

Figure 38: Profile image of the heat flow vector of the finite element random model.

Table 6: Comparison between random model and experimental result.

Model type	Thermal conductivity coefficient ($W \cdot m^{-1} \cdot K^{-1}$)		
	A	B	C
Random model	0.4422	0.4633	0.4990
Experiment result	0.45	0.423	0.5
Deviation (%)	1.74	9.53	0.192

(3) The thermal conductivity coefficient results of the cross-linked model are in good agreement with the experimental results, which can well predict the heat transfer characteristics of the actual carbonization layer

(4) The thermal conductivity coefficient of the finite element random model is in good agreement with the experimental results and has higher precision than the double scale model, proving that the established FEM model is in good agreement with the actual heat transfer behavior

Data Availability

The data used to support the findings of this study are included within the article.

Conflicts of Interest

The authors declare that they have no conflicts of interest.

Acknowledgments

The authors acknowledge the fund support from the State Key Basic Research and Development Plan (2015CB655201).

References

[1] M. Stackpoole, S. Sepka, I. Cozmuta, and D. Kontinos, "Post-flight evaluation of stardust sample return capsule forebody heatshield material," in *46th AIAA Aerospace Sciences Meeting and Exhibit*, vol. 1202, p. 12, Reno, Nevada, January 2008.

[2] S. Q. Zeng, A. Hunt, and R. Greif, "Geometric structure and thermal conductivity of porous medium silica aerogel," *Journal of Heat Transfer*, vol. 117, no. 4, pp. 1055–1058, 1995.

[3] Z. S. Cheng, J. Qian, and Y. H. Ye, "Theoretical calculation of equivalent thermal conductivity of composites," *Journal of University of Science and Technology of China*, vol. 22, no. 4, pp. 416–424, 1992.

[4] G. D. Cheng and S. T. Liu, "Prediction of thermal conductivity of unidirectional fiber composites," *Acta Mareriae Composite Sinica*, vol. 13, no. 1, pp. 78–85, 1996.

[5] F. A. Al-Sulaiman, E. M. A. Mokheimer, and Y. N. Al-Nassar, "Prediction of the thermal conductivity of the constituents of fiber reinforced composite laminates," *Heat and Mass Transfer*, vol. 42, no. 5, pp. 370–377, 2006.

[6] J. K. Farooqi and M. A. Sheikh, "Finite element modelling of thermal transport in ceramic matrix composites," *Computational Materials Science*, vol. 37, no. 3, pp. 361–373, 2006.

[7] B. Xia and Z. X. Lu, "Finite element analysis of thermophysical properties of 3D braided composites," *Acta Aeronautica et Astronautica Sinica*, vol. 32, no. 6, pp. 1040–1049, 2011.

[8] W. Luo, Z. Huang, C. Huang, M. Xiong, and S. Fan, "Numerical simulation of equivalent thermal conductivity of composite foam," *Journal of Wuhan University of Technology*, vol. 37, no. 12, pp. 12–16, 2015.

[9] S. Wang, G. He, J. Li, and Z. Liu, "Analysis of the structure characteristics of EPDM thermal insulation materials in a pure thermal chemical ablation environment," *Solid Rocket Technology*, vol. 33, no. 2, pp. 214–217, 2010.

[10] J. Chen, J. Li, Q. Li et al., "The structure characteristics of the carbonization layer of EPDM insulation material and its effect on ablation," *Solid Rocket Technology*, vol. 34, no. 1, pp. 122–125, 2011.

[11] Y. H. Xu, C. B. Hu, and J. Li, "Experimental study on the damage characteristics of the carbonization layer of EPDM insulation materials under particle erosion," *Engineering Mechanics*, vol. 28, no. 5, pp. 251–256, 2011.

[12] R. Fang and Q. W. Xu, "The influence of resin matrix on the structure of carbonized layer and fire-retardant properties of coatings," *Journal of Minjiang College*, vol. 28, no. 2, pp. 84–87, 2007.

[13] Y. Xu, C. Hu, Z. Zeng, and Y. Yang, "Study on the structure and characterization of the carbonized layer of EPDM insulation materials," *Journal of Missile and Guidance*, vol. 32, no. 3, pp. 237–242, 2012.

[14] H. P. Xu, *Study on the Properties of Carbonization Layer of Thermal Insulation Materials*, Inner Mongolia University, 2010.

[15] L. C. Sun, *Thermal Degradation and Laminated Flame-Retardant Properties of Wood - Plastic Composites*, Northeast Forestry University, 2016.

[16] S. Yang, G. He, J. Li, Q. Li, X. Sun, and S. Hu, "EPDM ablation model of loose/dense structure of carbonized layer," *Journal of Aerospace Power*, vol. 27, no. 5, pp. 1172–1178, 2012.

[17] S. X. Wang, "Analysis of pore structure and ablation gas state of thermal insulation material," *Weapons Materials Science and Engineering*, vol. 38, no. 4, pp. 48–51, 2015.

[18] R. E. Skochdopole, *The Thermal Conductivity of Foam Plastics*, vol. 57, Engineering Process, 1961.

[19] D. M. Curry, *An Analysis of a Charring Ablation Thermal Protection System*, National Aeronautics and Space Administration Houston TX Manned Spacecraft Center, 1965.

[20] J. Li, K. Xi, X. Lv, Q. Li, and S. X. Wang, "Characteristics and formation mechanism of compact/porous structures in char layers of EPDM insulation materials," *Carbon*, vol. 127, no. 2, pp. 498–509, 2018.

[21] L. G. Zhang, Z. Y. Ji, P. Y. He et al., "Effects of ultrasonic simulation on mechanical and release properties of alginate beads," *Journal of Beijing Technology University*, vol. 41, no. 9, pp. 1302–1307, 2015.

[22] P. He, J. Zhang, Z. Ji et al., ""Model analysis of mechanical properties of sodium alginate microspheres under ultrasonic thermal effect," *Journal of Military Medicine*, vol. 40, no. 12, 2016.

[23] J. Gao, J. Yu, H. Han, and D. Deng, "Prediction of meso-heat transfer characteristics of resin-based ablative materials," *Acta Aeronautica et Astronautica Sinica*, vol. 38, no. z1, pp. 170–177, 2017.

[24] G. R. Cunnington, C. A. Zierman, A. I. Funai, and A. Lindahn, *Performance of Multilayer Insulation Systems for Temperature to 700K*, Nasa Cr-907, 1967.

[25] S. F. Etris, V. K. Sisca, K. C. Lieb, I. C. Moore, A. L. Batik, and C. Bankvall, "Heat transfer in fibrous materials," *Journal of Testing and Evaluation*, vol. 1, no. 3, p. 235, 1973.